Lasers in Manufacturing Conference 2023

Holographic tuning of physical axicons

Jan Marx[a,*], Cemal Esen[a], Christian Lutz[b], Ralf Hellmann[b], Andreas Ostendorf[a]

[a] *Applied Laser Technologies, Ruhr University Bochum, Universitätsstr. 150, 44801 Bochum, Germany*
[b] *Applied Laser and Photonics Group, University of Applied Science Aschaffenburg, Würzburgerstr. 45, 63743 Aschaffenburg, Germany*

Abstract

Axicon generated Bessel beams are a popular tool for high aspect ratio precision laser drilling. Spot diameter and working distance are given by the geometric parameters of the axicon and the wavelength used. Thus, it is difficult to manipulate the beam shape of a Bessel beam for a given setup. Spatial light modulators (SLMs) overcome limitations in flexibility. However, due to the limited phase shift of SLMs, only Bessel beams with flat cone angles and large focal length can be generated. In this contribution, an approach for generating Bessel beams with a shorter, but tunable focal length is presented. A physical axicon was combined with an SLM. A holographic image of a negative axicon is put on the SLM to generate a ring beam, which is focused by a subsequent physical axicon to get a small focal diameter. Thus, different sized high aspect ratio micro holes can be drilled without using any moving components.

Keywords: Bessel beam; micro drilling; axicon; spatial light modulator; beam shaping

1. Introduction

The development goals for modern laser processing systems are flexible applicability combined with time-efficient processing. Flexible beam movement and shaping as well as multi-beam processing are fundamental techniques to reach these goals. Therefore, a variety of optical devices, such as diffractive optical elements (DOEs), spatial light modulators, and scanner systems, are continuously being improved and combined to further increase process speed [1,2]. However, most of the techniques work fine using Gaussian beams, but problems occur when the beam shape changes to a Bessel beam, since its spatial intensity

* Corresponding author.

distribution is much more complex than Gaussian intensity distribution and requires more sophisticated design and adjustment of the optical setup.

Contrary to a Gaussian beam, the Bessel beam is a diffraction free solution of the Helmholtz equation [3]. Bessel beams are characterized by a small focus area and an extended depth of focus with self-reconstructing properties [4]. Thus, they are a powerful tool for high aspect ratio processes, such as micro drilling [5,6] or micro patterning surfaces with sharp contours [7]. The most common way to generate Bessel beams is using an axicon lens to transform a Gaussian beam into a diffraction limited Bessel beam. A 4f lens setup in the far field of the axicon can be used for further demagnification of the beam [8-10]. Despite all advantages there are some practical issues when using Bessel beams in time efficient manufacturing processes. First, the center of the axicon and all subsequent lenses must be precisely aligned with the laser beam axis. The huge impact of small deviation of the axicon position not only causes a more complicated alignment of the laser setup, but it also makes it difficult to use a single axicon for multispot applications. Second, the usage of a galvano scanner for processing with Bessel beams is challenging. A scanner must not be placed in the long focal region of the Bessel beam to prevent damage on its mirrors caused by the high intensity of the central spot of the Bessel beam. Behind the focal region, the Bessel beam transforms into a ring beam, that can be refocused to a Bessel beam by convex lenses, but its diverging character must be considered when choosing subsequent optics. Third, the focus diameter of the Bessel beam only depends on the laser wavelength and the axicon angle as well as its refractive index [5]. Thus, it cannot be changed during process, which is a further limitation compared to Gaussian beam processing.

Over the years, many approaches have been developed to overcome the above-mentioned issues. Schwarz et al. [11] manufactured glass axicon arrays to generate high quality multi-Bessel beams. Their approach can really help to speed up Bessel beam material processing, but still their arrangement and focal spot diameter is fixed given by the geometry of the optics. An optical setup with adjustable diameter of the Bessel beam spot was described by Tiwari et al. [12] as well as Vaičaitis et al. [13]. They presented different optical setups where tuning of the spot size was done by adjusting the distance between the optics. An optical setup with variable Bessel spot size and without moving optical components was presented by Milne et al. [14]. They reported on a fluid-filled transitive axicon. An adjustment of the spot diameter can be done by changing the fluid by another one with a different diffraction index. However, processes with moving optics or exchange of fluids are quite slow. Higher process dynamics can be achieved by using spatial light modulators (SLMs). Almost any arbitrary intensity distribution can be reached by applying the right hologram. Thus, also, the generation of Bessel beams by an SLM has been reported many times [15-17]. Even multi-Bessel beams can be generated by superimposing holograms [18]. All SLM-generated Bessel beams are characterized by flat crossing angles resulting in large propagation length in the range of one meter and above. Although large focus depth Bessel beams can be demagnified by subsequent telescope optics, the integration of SLM-based Bessel beam optics in high power laser material processing systems is difficult due to the spatial extend. Even a convolution of the beam path by mirrors is not possible due to the high intensity of the focal spot.

Thus, a more compact solution of a tunable multi-Bessel spot drilling setup is presented in this paper. Therefore, a holographic axicon is combined with a physical axicon lens. The applicability of holographic beam splitters for multi-Bessel spot generation using a physical axicon was already proven in prior work [19, 20]. Here, we present further development of the former presented approach towards a multi-Bessel beam drilling optics with individual tuning of each focal spot diameter. Therefore, the beam splitter hologram can be superimposed with a hologram for a negative axicon for each sub-spot. Negative axicons are known to generate ring beams [21]. This was also proven by Zhai et al. for holographic negative axicons [22]. Contrary to positive axicons, there is no Bessel profile, thus no high intensity focal line in the nearfield behind the optics. When the modulated ring beam is imaged on the physical axicon, a resulting Bessel beam with a

crossing angle depending on both, holographic and physical axicon angle, is generated. The mathematical theory as well as results from drilling experiments are presented in the following sections.

2. Theoretical considerations and hologram generation

The spot diameter of a Bessel beam only depends on the laser wavelength λ and the crossing angle of the conical wavefront β [5]:

$$d_s = \frac{1.75 \cdot \lambda}{\pi \cdot \sin(\beta)} \qquad (1)$$

The geometry is shown in Figure 1a. For a physical Axicon, the crossing angle β_{phys} can be calculated using the law of refraction:

$$\beta_{phys} = (90° - \alpha) - \arccos\left(n \cdot cos(90° - \alpha)\right) \qquad (2)$$

With α and n being the cone angle of the axicon and its refractive index, respectively.

A similar consideration can be done for holographic axicons. Holograms for Bessel beams show concentric rings with linear phase shift, as shown in Figure 1b. The width of the rings can be described by a multiple of the SLMs pixel pitch. Typically, the maximum phase shift φ_{max} of SLMs is 2π, which equals one wavelength. Thus, a relation between the width of the rings and a theoretical crossing angle of the holographic Bessel beam β_{hol} can be calculated with equation 3, where p is the number of pixels within the width of one ring:

$$\beta_{hol} = \frac{\lambda}{p \cdot pixelpitch} \qquad (3)$$

It can be seen that high crossing angles require narrow rings with few pixels. As Lingel et al. [23] observed, a smaller grating period reduces the diffraction efficiency of the hologram. Thus, the pixel size of the SLM determines the maximum axicon angle and the minimum spatial extend of the interfering zone, respectively.

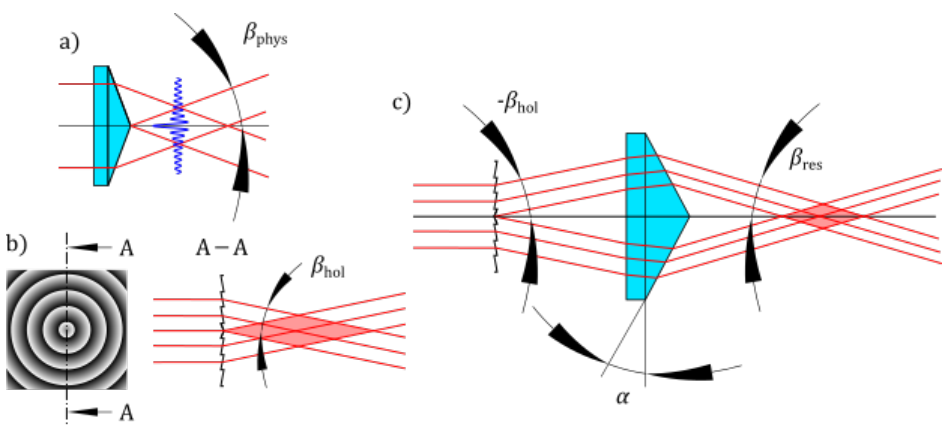

Fig. 1. a) Beam path of a physical axicon. The blue line indicates the radial intensity distribution. b) Hologram of an SLM-generated axicon and its beam path. c) Combination of a holographic negative axicon and a physical axicon. For better clarity, the SLM is shown with transmissive, instead of reflective behavior in this figure.

An inversion of the hologram image changes the sign of β_{hol}. A negative crossing angle results in a ring beam without an interfering region on the optical axis [21]. When such a ring beam is projected onto a physical axicon (Figure 1c), the holographic crossing angle and the physical crossing angle are summed up to a resulting crossing angle (assuming small angles and negligible refraction at the entrance surface of the axicon):

$$\beta_{hol} + \beta_{phys} = \beta_{res} \qquad (4)$$

By changing the holographic crossing angle, it is possible to adjust the spot diameter while the resulting focus length can be kept short. However, this tunable axicon variant still requires additional elements for a flexible generation of multispot patterns. In the following, the angle $-\beta_{hol}$ is defined as tuning angle.

By adding up a linear blazed grating to the negative axicon hologram, the resulting ring beam gets deflected. Since the beam must be aligned to the center of the axicon, a convex lens must be placed between the SLM and the subsequent physical axicon to image the modulated beam onto the center of the axicon. Detailed investigations on the characteristics of the beam shaping setup can be found in prior work [20]. Most importantly, adding a lens in front of the physical axicon makes the beam divergent. Thus, equation 4 is not matched perfectly anymore and also, the resulting Bessel beam behind the physical axicon is slightly divergent. However, the resulting axicon angle can still be tuned by the holographic negative axicon. The following parameter variation shows that the tuning effect is even enhanced by the additional lens between the holographic and the physical axicon. Multiple deflected Bessel spots were superimposed using the prism and lens algorithm described by Liesener et al. [24]. The described method allows to generate multiple Bessel spots with different spot diameter for each of them. In the following, the applicability of this method was verified by performing drilling experiments.

3. Experimental setup

The experiments have been carried out using an ultrashort pulsed 800 nm Ti:Sa-laser (Spitfire Ace, Spectra-Physics). The beam path is shown in Figure 2. The minimum pulse width of the raw beam was measured at 110 fs by using an autocorrelator (APE Mini, Angewandte Physik & Elektronik GmbH). The internal pulse stretcher-compressor system was used to counteract the pulse dispersion caused by the beam shaping optics. The power adjustment of the laser beam was realized by combining a half-waveplate with a polarizing beam splitter. The 8.3 mm raw beam of the laser was demagnified by a telescope (f_1 = 250 mm and f_2 = -150 mm) to 5.1 mm before it hits the reflective SLM (Pluto 2, Holoeye, pixel pitch 8 µm) to make sure there is almost no reflection outside the active area on the SLM. The maximum pulse energy, that can be applied to the SLM, is 200 µJ. Behind the SLM, the modulated beam passes a bi-convex lens (f_3 = 75 mm) for imaging the phase hologram on the subsequent axicon (cone angle α = 2°). A telescope for further demagnification of the beam was placed in the far field of the axicon (f_4 = 300 mm, f_5 = 25 mm). The distance between the axicon and the lens f_4 is given by the half propagation length of an untuned Bessel beam (z_{max} / 2 = 78.5 mm) plus the focal length of the lens.

20 µm thick steel foils (material No. 1.1274) were used as samples. An argon gas flow (8 l/min) through a gas nozzle was used to reduce oxidation of the sample surface during the process. The samples were mounted on an xyz-stage (M-521.DD for x- and y-axis, M-511.DG for z-axis, Physik Instrumente (PI)) for positioning. The stage was not moved during single drilling experiments, all relative movements between beam and sample were achieved holographically by the SLM. Due to the slightly diverging character of the Bessel beam, the scan field for the beam deflection can be adjusted by changing the axial position of the

sample. Thus, the samples surface was placed 3 mm behind the theoretical focal point of the objective lens for having an enlarged scan field for the holographically deflected beams.

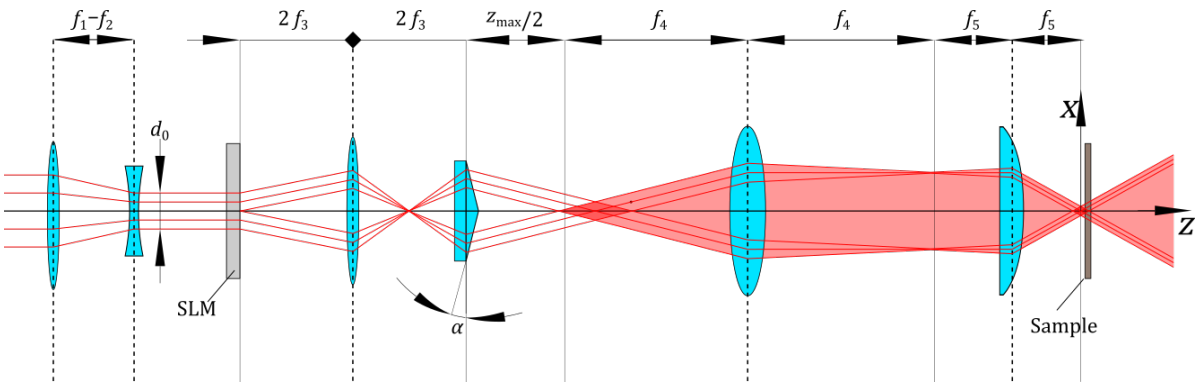

Fig. 2. Experimental setup with all beam shaping elements along the beam path: telescope (f_1 = 250 mm, f_2 = -150 mm) demagnifying the beam to a diameter of d_0 = 5.1 mm, reflective SLM (the transmittive representation in this figure serves the clarity), imaging lens (f_3 = 75 mm), axicon (α = 2°, Bessel beam propagation length of untuned beam z_{max} = 157 mm), the second telescope (f_4 = 300 mm, f_5 = 25 mm), sample placed 3 mm behind the focus of f_5 (The figure is not true to scale).

Characterization of the samples was performed using a scanning electron microscope (SEM, EVO MA10, Zeiss). A transmitted light microscope (Eclipse LV 1000, Nikon) was used to detect the perforation of the samples.

4. Results

Two sets of experiments were carried out: First, the Bessel beam was just tuned by applying the hologram of a negative axicon to the SLM. Second, blazed gratings were added to generate double spots with different sized focal diameter.

4.1. Single spots

In this section, the crossing angle of the holographic axicon was varied between 0° (which means the SLM shows a constant phase) and -0.5° in steps of 0.02°. Five drilling processes were carried out with each hologram. All experiments were carried out using a pulse energy of 100 µJ and the sample was exposed for 1 s at a repetition rate of 500 Hz. Figure 3 shows some representative SEM images of the results.

As expected, the bore holes drilled with the Bessel beam tuned by a negative holographic axicon show larger spot diameter. However, the broader focal spot is accompanied by lower fluence. Thus, only experiments with negative holographic axicons up to a tuning angle of 0.26° led to through holes. The diameter of the ablation of the central core d_c of the Bessel beam was measured and is shown in Figure 4. As mentioned above, the diameter of the Bessel beam as well as the intensity affect the ablation diameter. Thus, the diameter of the Bessel beam cannot be determined solely by the central ablation diameter. Therefore, the diameter of the first d_{r1} and second d_{r2} order ring around the central core of the Bessel beam was also measured. By measuring the distance at half width of the ring (see Figure 3a), the distance only depends on the spatial geometry of the Bessel beam and not on the total intensity. However, ablation by the higher order rings can be seen just up to a tuning angle of 0.22° (second order ring) and 0.40° (first order ring), respectively. A comparison between the diameter of the first order ring without tuning (⌀33 µm) and

with a tuning angle of 0.4° (⌀65 µm) shows, that the diameter of the Bessel profile can be enlarged by almost 100 % within the tuning range.

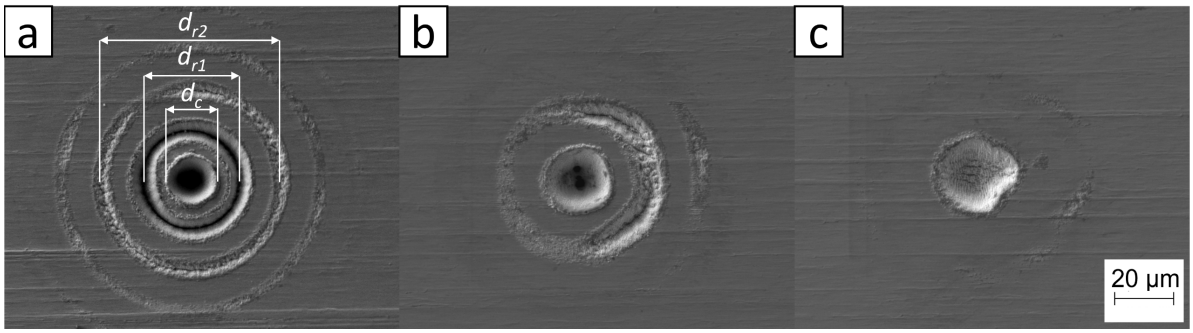

Fig. 3. Comparison of bore holes processed with (a) an untuned axicon and with a tuning angle of (b) 0.26° and (c) 0.44°.

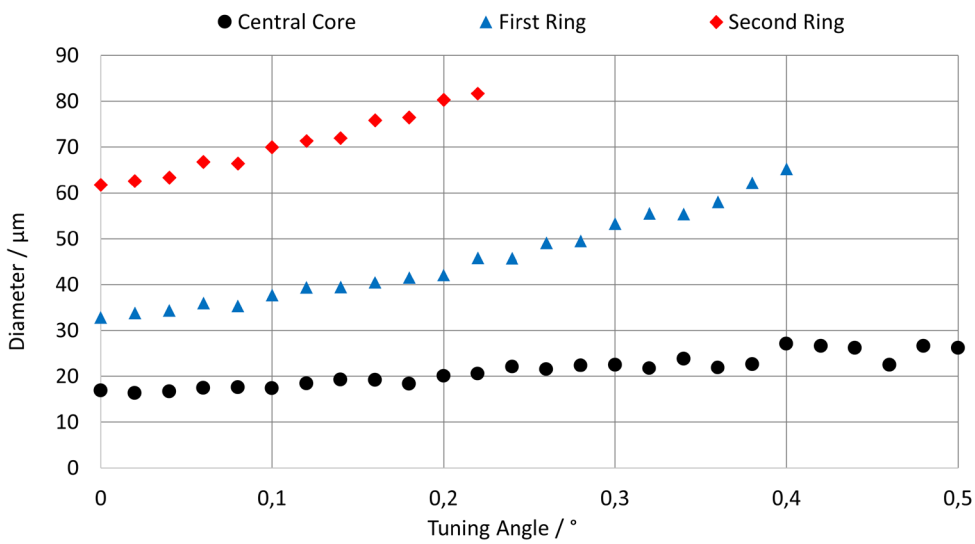

Fig. 4. Diameter of the central core of the ablation, the first ring, and the second ring at different tuning angles. The standard deviation of all measured diameters is below 0.8 µm.

With respect to the diagram in Figure 4, two deviations from the expected results can be observed. First, the graphs for the ring diameter should be linear, according to equation 4. Instead, there is a slightly progressive trend that is assumed to be due to the lens in front of the axicon, which makes the Bessel beam slightly divergent. Second, there are some outliers for the central core ablation diameter in Figure 4. A random process deviation can be excluded, since the standard deviation of all measured diameters is < 0.8 µm, thus, far below the deviation of the outliers. However, the outliers only occur at high tuning angles. The most striking one is at a tuning angle of 0.46°. At this point, the rings of the hologram consist of only 12 or 13 pixels. Thus, the rounding error due to the discrete pixel number will have a non-negligible influence on the diffracted image.

4.2. Multi spots

To demonstrate drilling processes with different sized holes at one time, a beam splitting hologram was added to the SLM to create double spots. A negative axicon is superimposed to change the crossing angle of one of the two spots. The grating separating the spots was symmetrical and had a deflection angle of ±0.1°. The separation distance between the spots was 125 µm at the sample surface. The pulse energy was 200 µJ. Thus, assuming an equal distribution of energy to both spots, there is still the same energy applied to each borehole compared to the experiments in the former section.

The SEM images of the double drillings show some more complex microstructures than in single Bessel beam experiments. Around the central core of the ablation there are no longer rings, but a non-circular pattern. The pattern can be related to interference effects between the two beams, which were already observed in former experiments [20]. Nevertheless, the core ablation of both beams can be seen clearly and the differences in diameter are obvious. The diagram of the hole diameter (Figure 5d) shows some more irregularities compared to the former section. The irregularities are not exclusively attributed to the pixel size, but also to interference effects between the Bessel beam core of the one beam and the higher order rings of the other beam. This effect can be seen very clearly at a tuning angle of 0.38° (Figure 5c), where the effect leads to a broadening of the ablated area. Since the interference effects cause elliptically shaped holes in some cases, the hole diameter displayed in Figure 5d are averaged values between the long and short axis.

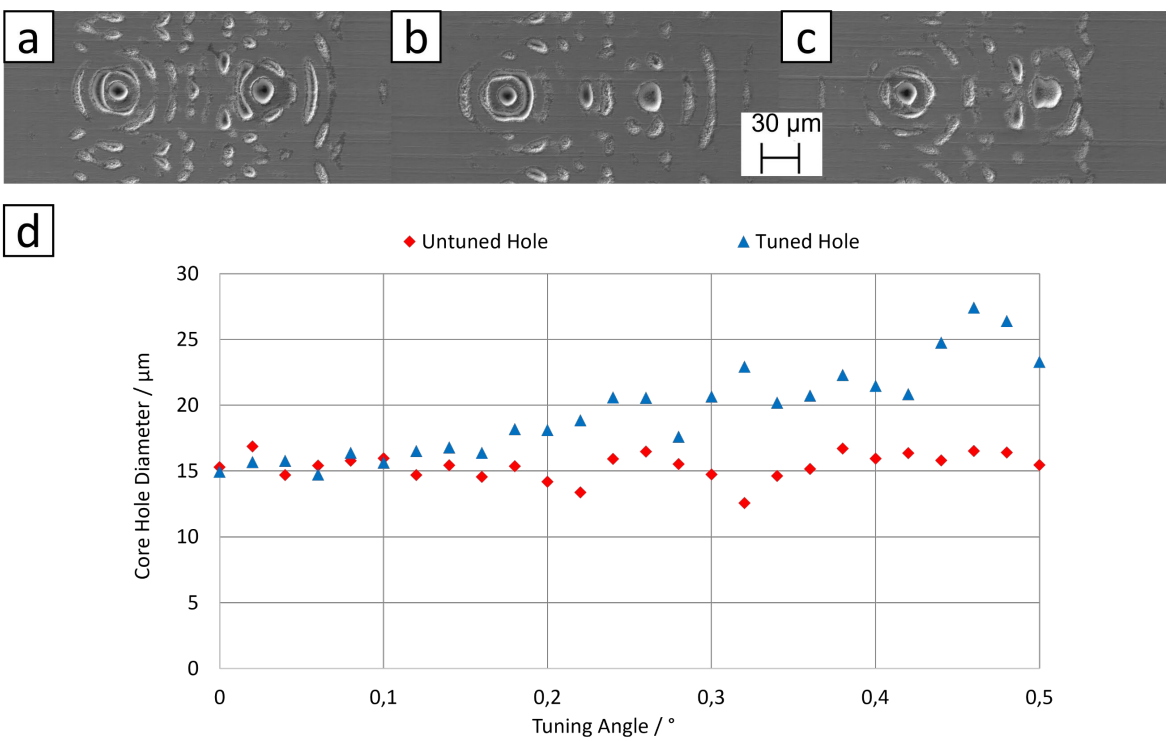

Fig. 5. SEM images at tuning angles of a) 0.2°, b) 0.34°, and c) 0.38°; d) Bessel core ablation diameter of the tuned hole and untuned hole at different tuning angles. The standard deviation at all parameters is below 1.1 µm.

5. Conclusion and outlook

A new method for flexible adjustment of Bessel beam spot diameter based on the combination of a physical axicon and an SLM was successfully demonstrated. Characterization of ablation experiments using the higher order rings of the Bessel beam showed, that the radial extend of the Bessel beam profile can be doubled within a tuning range of 0.4°. The presented setup shows a good compromise between rapid beam adjustment, flexibility in changing the spot diameter and a compact and robust design. Nevertheless, precise adjustment of the laser pulse energy is mandatory for good drilling results. The resulting ablation diameter not only depends on the tuned axicon angle, but also changing the applied fluence due to changing spot diameter, changing diffraction efficiency at different tuning angles and interference effects between multispots. A future research aspect will be to find rules how to calculate the needed pulse energy taking all these aspects into account.

Acknowledgements

We gratefully acknowledge funding by the German Federal Ministry for Economic Affairs and Climate Action under grant 16KN053050.

References

[1] M. Gafner, S. Remund, M. V. Chaja, T. Mähne, B. Neuenschwander, Ultrafast stamping by combination of synchronized galvanometer scanning with DOE's or SLM, Procedia CIRP 94 (2020) 802–806. https://doi.org/10.1016/j.procir.2020.09.126.

[2] L. Ackermann, M. Gehring, C. Roider, K. Cvecek, M. Schmidt, Spot arrays for uniform material ablation with ultrashort pulsed lasers, Optics & Laser Technology 163 (2023) 109358. https://doi.org/10.1016/j.optlastec.2023.109358.

[3] J. Durnin, J. J. Miceli, J. H. Eberly, Diffraction-free beams, Physical Review Letters 58 (1987) 1499–1501. https://doi.org/10.1103/PhysRevLett.58.1499.

[4] D. McGloin, K. Dholakia, Bessel beams: Diffraction in a new light, Contemporary Physics 46 (2005) 15–28. https://doi.org/10.1080/0010751042000275259.

[5] Y. Matsuoka, Y. Kizuka, T. Inoue, The characteristics of laser micro drilling using a Bessel beam, Applied Physics A 84 (2006) 423–430. https://doi.org/10.1007/s00339-006-3629-6.

[6] I. Alexeev, K.-H. Leitz, A. Otto, M. Schmidt, Application of Bessel beams for ultrafast laser volume structuring of non transparent media, Physics Procedia 5 (2010) 533–540. https://doi.org/10.1016/j.phpro.2010.08.177.

[7] J. Marx, J. Tenkamp, F. Walther, C. Esen, Fabrication of Rectangular Micro-Channels, Journal of Laser Micro/Nanoengineering 17 (2022). https://doi.org/10.2961/jlmn.2022.03.2003.

[8] D. Grojo, A. Mouskeftaras, P. Delaporte, S. Lei, Limitations to laser machining of silicon using femtosecond micro-Bessel beams in the infrared, Journal of Applied Physics 117 (2015) 153105. https://doi.org/10.1063/1.4918669.

[9] Q. Xie, X. Li, L. Jiang, B. Xia, X. Yan, W. Zhao, Y. Lu, High-aspect-ratio, high-quality microdrilling by electron density control using a femtosecond laser Bessel beam, Applied Physics A 122 (2016) 136. https://doi.org/10.1007/s00339-016-9613-x.

[10] T. Chen, G. Zhang, Y. Wang, X. Li, R. Stoian, G. Cheng, Reconstructing of Embedded High-Aspect-Ratio Nano-Voids Generated by Ultrafast Laser Bessel Beams, Micromachines 11 (2020) 671. https://doi.org/10.3390/mi11070671.

[11] S. Schwarz, S. Rung, C. Esen, R. Hellmann, Rapid fabrication of precise glass axicon arrays by an all laser-based manufacturing technology, Journal of Laser Applications 32 (2020) 12001. https://doi.org/10.2351/1.5134988.

[12] S.K. Tiwari, S.R. Mishra, S.P. Ram, H.S. Rawat, Generation of a Bessel beam of variable spot size, Applied optics 51 (2012) 3718–3725. https://doi.org/10.1364/AO.51.003718.

[13] V. Vaičaitis, Š. Paulikas, Formation of Bessel beams with continuously variable cone angle, Optical and quantum electronics 35 (2003) 1065–1071. https://doi.org/10.1023/A:1026096305442.

[14] G. Milne, G. D. M. Jeffries, D. T. Chiu, Tunable generation of Bessel beams with a fluidic axicon, Applied physics letters 92 (2008) 261101. https://doi.org/10.1063/1.2952833.

[15] I. A. Litvin, T. Mhlanga, A. Forbes, Digital generation of shape-invariant Bessel-like beams, Optics express 23 (2015) 7312–7319. https://doi.org/10.1364/OE.23.007312.

[16] C. Vetter, R. Steinkopf, K. Bergner, M. Ornigotti, S. Nolte, H. Gross, A. Szameit, Realization of Free-Space Long-Distance Self-

Healing Bessel Beams, Laser & Photonics Reviews 13 (2019) 1900103. https://doi.org/10.1002/lpor.201900103.
[17] L. Stoyanov, Y. Zhang, A. Dreischuh, G. G. Paulus, Long-range quasi-non-diffracting Gauss-Bessel beams in a few-cycle laser field, Optics express 29 (2021) 10997–11008. https://doi.org/10.1364/OE.419486.
[18] R. Bowman, N. Muller, X. Zambrana-Puyalto, O. Jedrkiewicz, P. Di Trapani, M.J. Padgett, Efficient generation of Bessel beam arrays by means of an SLM, The European Physical Journal Special Topics 199 (2011) 159–166. https://doi.org/10.1140/epjst/e2011-01511-3.
[19] C. Lutz, S. Schwarz, S. Rung, J. Marx, C. Esen, R. Hellmann, Optical system for multi Bessel beam high power ultrashort pulsed laser processing using a spatial light modulator, Lasers in Manufacturing-LiM 2021 (2021).
[20] J. Marx, C. Lutz, R. Hellmann, C. Esen, Holographic multi-spot generation for ultra-short pulse Bessel beam processing of stainless steel, Procedia CIRP 111 (2022) 648–652. https://doi.org/10.1016/j.procir.2022.08.003.
[21] S. Schwarz, G.-L. Roth, S. Rung, C. Esen, R. Hellmann, Fabrication and evaluation of negative axicons for ultrashort pulsed laser applications, Optics express 28 (2020) 26207–26217. https://doi.org/10.1364/OE.401084.
[22] Z. Zhai, Z. Cheng, Q. Lv, X. Wang, Tunable Axicons Generated by Spatial Light Modulator with High-Level Phase Computer-Generated Holograms, Applied Sciences 10 (2020) 5127. https://doi.org/10.3390/app10155127.
[23] C. Lingel, T. Haist, W. Osten, Optimizing the diffraction efficiency of SLM-based holography with respect to the fringing field effect, Applied optics 52 (2013) 6877–6883. https://doi.org/10.1364/AO.52.006877.
[24] J. Liesener, M. Reicherter, T. Haist, H.J. Tiziani, Multi-functional optical tweezers using computer-generated holograms, Optics Communications 185 (2000) 77–82. https://doi.org/10.1016/S0030-4018(00)00990-1.